Appendix A: Supplementary Material

Title: Co-precipitation induces changes to carbon and iron chemistry and spatial distribution at the nanometer scale

Authors:
Possinger, Angela R.[1#]
Zachman, Michael J.[2##]
Dynes, James J.[3]
Regier, Tom Z.[3]
Kourkoutis, Lena F.[2,4]
*Lehmann, Johannes[1,5,6]
1. School of Integrative Plant Science, Section of Soil and Crop Sciences, Cornell University
2. School of Applied and Engineering Physics, Cornell University
3. Canadian Light Source, Saskatoon, SK
4. Kavli Institute at Cornell for Nanoscale Science, Cornell University
5. Cornell Atkinson Center for Sustainability, Cornell University
6. Institute for Advanced Studies, Technical University Munich, Garching, Germany
*Corresponding author, Email: CL273@cornell.edu
#Current address: Virginia Tech, Department of Forest Resources and Environmental Conservation
##Current address: Center for Nanophase Materials Sciences, Oak Ridge National Laboratory

A1. Supplementary Methods

A1.1 Iron K-edge XANES Model

To describe the shift in energy associated with Fe(II), we used an Fe K-edge X-ray absorption near-edge structure (XANES) model modified from Inagaki et al. (2020) and Possinger et al. (2020a). In this study, we used four non-negative Gaussian functions with varying height, energy position, for Gaussian functions at ~7112 (pre-edge centroid), 7117-7120, 7124, and 7128 eV. The function at the ~7117-7120 eV energy position was constrained to ~7118 ± 3*sin(~0). The FWHM of all functions was constrained to 2eV ± 2*sin(~0). The model was fit in Fityk v. 0.9.8 (Wojdyr, 2010) using the Levenberg-Marquardt algorithm with 1000 maximum iterations to minimize the maximum sum of squared residuals (MSSR). The relative change in spectral shape associated with increasing Fe(II) was estimated by the proportion of 7117-7120 eV area as a function of total Gaussian area. This approach emphasizes relative changes in Fe(II), rather than absolute abundance. The detection of increased 7117-7120 eV area in mixed Fe(II)/Fe(III) and predominantly Fe(II) minerals only suggests that the XAS analysis did not systematically induce Fe(II) damage artifacts (Supplementary Fig. A3.10).

A1.2 Cryogenic STEM-EELS Damage Assessment

Electron energy loss spectroscopy (EELS) low-dose measurements (~10,000 and 67,000 electrons (e^-) $Å^{-2}$) from Possinger et al. (2020b) and measurements in this study (~100,000 to ~1,000,000 e^- $Å^{-2}$) were used to assess the presence of artifacts from increasing exposure on C K-edge and Fe $L_{2,3}$-edge EELS spectral fine structure

(Supplementary Figs A3.1-A3.2). For each image, average spectra were extracted using the Cornell Spectrum Imager (CSI) package (Cueva et al., 2012) in ImageJ v. 2.0.0 (Schneider et al., 2012). A standard linear combination of power laws (LCPL) approach was used to subtract the background signal with 3-pixel local background averaging. Differences in C K-edge and Fe $L_{2,3}$-edge region intensities as a function of dose were assessed by estimation of area under the curve (AUC) for aromatic C (284.5-285.5 eV), substituted aromatic C (286.0-287.0 eV), aliphatic C (287.0-287.5 eV), carboxylic C (287.8-289.0 eV), reduced Fe(II) (707.0-709.75 eV) and oxidized Fe(III) (709.75-712.5 eV). The AUC was estimated using the trapezoidal method in the "DescTools" package (Signorell et al., 2020) for R v. 4.0.2 (R Core Team, 2019) in RStudio v. 1.1.423 (RStudio Team, 2015). To interpret changes in AUC, we calculated Fe(II)/Fe(III) and (aromatic + substituted aromatic)/(aliphatic + carboxylic C) ratios, termed here lower/higher-energy ratios, respectively, for simplicity. In addition, the lower/higher-energy AUC ratio for Fe was compared between adsorbed and co-precipitated WEOM-Fe images collected at a similar dose (Supplementary Fig. A3.3).

A1.3 EELS Elemental Spatial Distribution

Elemental electron energy loss spectroscopy (EELS) maps of iron (Fe), carbon (C), nitrogen (N), and oxygen (O) in Site 1 water-extractable organic matter (WEOM)-ferrihydrite samples and Fe and C in Site 2 WEOM-ferrihydrite samples were used to assess spatial relationships between elements and the spatial aggregation patterns of Fe. Elemental maps were obtained by background-subtracting spectra and integrating edges with the Cornell Spectrum Imager (CSI) package (Cueva et al., 2012) in ImageJ

v. 2.0.0 (Schneider et al., 2012). A standard linear combination of power laws (LCPL) approach was used to subtract the background signal with 3-pixel local background averaging. Spatial analysis of maps was performed using R in RStudio. Non-sample area (vacuum) was manually filtered to avoid inflation of correlation estimates (Supplementary Figs A3.4-A3.5) and pixel intensity was normalized to maximum intensity = 1. Pixel intensity correlation between element pairs (Fe-C, Fe-N, and Fe-O) and C and Fe components was determined in base R in RStudio using Spearman Rank Correlation with asymptotic t approximation for p-values.

A1.4 Iron Distribution and Clustering

To determine the effect of co-precipitation on the spatial clustering of Fe relative to surface adsorption, elemental Fe maps were analyzed using the Ripley’s K(t) and Moran’s I functions using the “spatstat” (Baddeley et al., 2015) and “ape” (Paradis et al., 2004) R packages in RStudio. Ripley’s K(t) gives a distribution as a function of distance from randomly sampled points in a spatial point pattern, providing information on the distribution of features within an image. Ripley’s K(t) distributions were plotted in comparison to the Poisson distribution that is expected with a complete spatially random distribution; values above the Poisson distribution are considered clustered, while values below the Poisson distribution are considered evenly spaced (Baddeley et al., 2015). Ripley’s K(t) plots were generated using the border method for edge estimation and ~99% confidence envelopes. Moran’s I tests autocorrelation of Fe-contained pixels in each image. To meet the assumption of square image geometry for Ripley’s K analysis, the largest square area in filtered images used for elemental correlations was rescaled (intensity range 0 to 1) and converted to a binary image (pixel intensity >50% set to 1) (Supplementary Fig. A3.4-A3.5). Moran’s I autocorrelation was compared between co-precipitation and adsorption treatments using the Wilcoxon Rank Sum Test (base R in RStudio).

A2. Supplementary Results and Discussion

A1.2 Cryogenic STEM-EELS Damage Assessment

For both C and Fe, spectra did not vary systematically as a function of the applied dose (Supplementary Fig. A3.1A). In contrast, measurements made in spatially proximal regions of interest (ROI) accounted for the major differences in spectral fine structure (Supplementary Fig. A3.1B). Within a given ROI, the ratio of lower/higher-energy AUC in some cases increased with increasing dose (Supplementary Fig. A3.2). For C, this was driven mostly by decreased signal in the carboxylic region (287.8-289.0 eV) (Supplementary Fig. A3.1B). However, changes in lower/higher-energy AUC ratio were not consistent across all ROIs for either Fe or C (Supplementary Fig. A3.2).

For Fe, our measurements were conducted below the dose observed for room-temperature EELS formation of Fe(II) damage artifacts in ferrihydrite (3×10^6 e^- $Å^{-2}$) (Pan et al., 2006). This is further supported by the fact that our measurements were performed under cryogenic conditions, which can stabilize materials compared to measurement at room temperature (Kourkoutis et al., 2012; Miot et al., 2014). Additionally, the Fe(II)/Fe(III) AUC ratio of the L_3-edge was higher for co-precipitated WEOM-Fe at comparable dose and identical microscope conditions (Supplementary Fig. A3.3), highlighting that the presence of Fe(II) was treatment-dependent and not linked to damage artifacts. Additionally, we detected reduced Fe(II) MCR components in images varying in dose by a factor of 4.4 (Supplementary Table A4.5).

For C, decreased carboxylic intensity in the highest dose spectrum (measurement “i”, shown in detail in manuscript Figs. 4-6) may be influenced by beam exposure. This measurement was not collected with a paired lower-dose measurement in the same region; therefore, so we cannot definitively conclude whether sample location or beam exposure was the primary driver of the spectrum fine structure difference relative to the other measurements. However, AUC between this high-dose measurement and a sample region with similar properties (measurement “d”) differed by 26% at maximum, and less than 5% for carboxylic C, despite a 4.4 factor difference in applied dose (Supplementary Table A4.5). The spatial correlations (Spearman’s ρ) between total and lower-energy C and reduced Fe(II) components were also similar between these measurements (Supplementary Fig. A3.13).

Taken together, these observations suggest that carboxylic C may be more sensitive to beam damage than other C components, but that our interpretations are not driven by carboxylic C beam damage artifacts. However, to avoid overinterpretation of subtle differences in spectral features, we limited interpretation of the co-precipitate EELS data shown in main text Figs 4-6 and Supplementary Fig. A3.13 to generalized energy regions of statistically-resolved MCR components (note that a well-resolved lower-energy MCR component was identified in all co-precipitated samples, regardless of dose, as shown in manuscript Fig. 4A). Moreover, spatial correlations of MCR components defined as “lower- and higher-energy C” were used, rather than differences in individual peak height or variations in specific bonding environments (i.e., functional groups).

A2.2 Chemical Composition of WEOM: Rationale for Pooled Observations

Water-extractable organic matter (WEOM) used in this study was collected for the co-precipitation and adsorption experiments from two sites on a hillslope transect. The upslope, “E” podzol site (Site 2) had slightly higher coniferous basal area (35% vs 0% for the sampling area) than the “typical” site (Site 1) (Possinger et al., 2020a). However, basal area was dominated by the same deciduous species (*Betula alleghaniensis*), and throughout the course of the experiment, no appreciable differences in WEOM composition (via C K-edge XANES), co-precipitate or adsorption C content, or bulk co-precipitate vs. adsorption sample XAS (Fe or C) associated with WEOM source were detected. Co-precipitate and adsorption complex C:Fe molar ratio was adjusted to 10:1 for both WEOM sources, accounting for differences in the initial C content. Consequently, the interpretations on the spatial and compositional changes between co-precipitation and adsorption were therefore pooled with respect to WEOM source.

References

Baddeley A., Rubak E. and Turner R. (2015). *Spatial Point Patterns: Methodology and Applications with R*. Chapman and Hall/CRC Press, London.

Chen C., Dynes J. J., Wang J. and Sparks D. L. (2014). Properties of Fe-organic matter associations via coprecipitation versus adsorption. *Environ. Sci. Technol.* **48**, 13751-13759.

Chen K., Chen T., Chan Y., Cheng C., Tzou Y., Liu Y. and Teah H. (2016). Stabilization of natural organic matter by short-range-order iron hydroxides. *Environ. Sci. Technol.* **50**, 12612-12620.

Cueva P., Hovden R., Mundy J. A., Xin H. L. and Muller D. A. (2012). Data processing for atomic resolution electron energy loss spectroscopy. *Micros. Microanal.* **18**, 667-675.

Heymann K., Lehmann J., Solomon D., Schmidt M. W. I. and Regier T. (2011). C 1s K-edge near edge X-ray absorption fine structure (NEXAFS) spectroscopy for characterizing functional group chemistry of black carbon. *Org. Geochem.* **42(9)**, 1055-1064.

Inagaki T. M, Possinger A. R., Grant K. E., Schweizer S. A., Mueller C. W., Derry L. A., Lehmann J. and Kögel-Knabner I. (2020). Subsoil organo-mineral associations under contrasting climate conditions. *Geochim. Cosmochim. Acta* **270**, 244-263.

Kourkoutis L. F., Plitzko J. M. and Baumeister W. (2012). Electron microscopy of biological materials at the nanometer scale. *Annu. Rev. Mater. Res*. **42**, 33-58.

Miot J., Benzerara K. and Kappler A. (2014). Investigating microbe-mineral interactions: recent advances in X-ray and electron microscopy and redox-sensitive methods.

Annu. Rev. Earth Planet. Sci. **42**, 271-289.

Pan Y., Brown A., and Brydson R. (2006). Electron beam damage studies on 6-line ferrihydrite. *J. Phys. Conf. Ser.* **26**, 46-49.

Paradis E., Claude J. and Strimmer K. (2004). APE: analyses of phylogenetics and evolution in R language. *Bioinformatics* **20**, 289-290.

Possinger A. R., Bailey S. W., Inagaki T. M., Kögel-Knabner I., Dynes J. J., Arthur Z. A. and Lehmann J. (2020a). Organo-mineral interactions and soil carbon mineralizability with variable saturation cycle frequency. *Geoderma* **375**, 114883.

Possinger, A. R., Zachman, M. J., Enders, A., Levin, B. D. A., Muller, D. A., Kourkoutis, L. F. and Lehmann, J. (2020b). Organo-organic and organo-mineral interfaces in soil at the nanometer scale. *Nat. Commun.* **11**, 6103.

RStudio Team (2015). RStudio: Integrated Development for R. RStudio, Inc., Boston. URL http://www.rstudio.com/

R Core Team (2019). R: A language and environment for statistical computing. R Foundation for Statistical Computing, Vienna, Austria. URL https://www.R-project.org/.

Schneider C. A., Rasband W. S. and Eliceiri K. W. (2012). NIH Image to ImageJ: 25 years of image analysis. *Nature Methods* **9(7),** 671-675.

Signorell, A. et al. (2020). DescTools: Tools for descriptive statistics. R package version 0.99.37.

Wojdyr M. (2010). Fityk: a general-purpose peak fitting program. *J. Appl. Cryst.* **43**, 1126-1128.

A3. Supplementary Figures

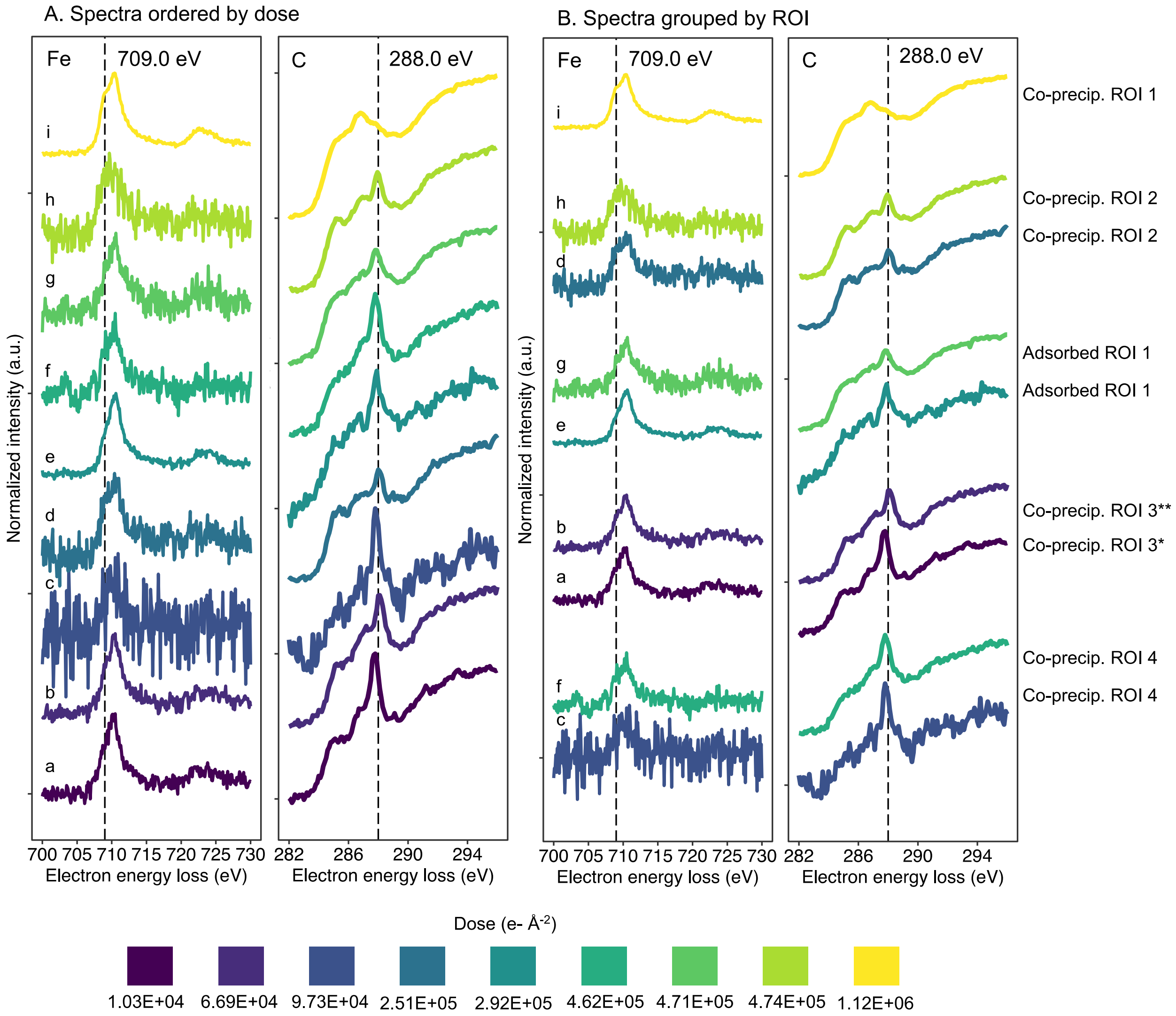

Supplementary Fig. A3.1. Iron (Fe) and carbon (C) electron energy loss spectra sorted by dose (**A**) or grouped by proximal regions of interest (ROI) within each sample (**B**). Low-dose measurements (spectra "a" and "b") were conducted on co-precipitated water-extractable organic matter (WEOM)-iron (Fe) samples with increasing dose via increasing exposure time on the same sample area (* = 10 and ** = 70 s) (Possinger et al., 2020b). Spectra "a" through "i" correspond to measurement parameters described in Supplementary Table A4.4.

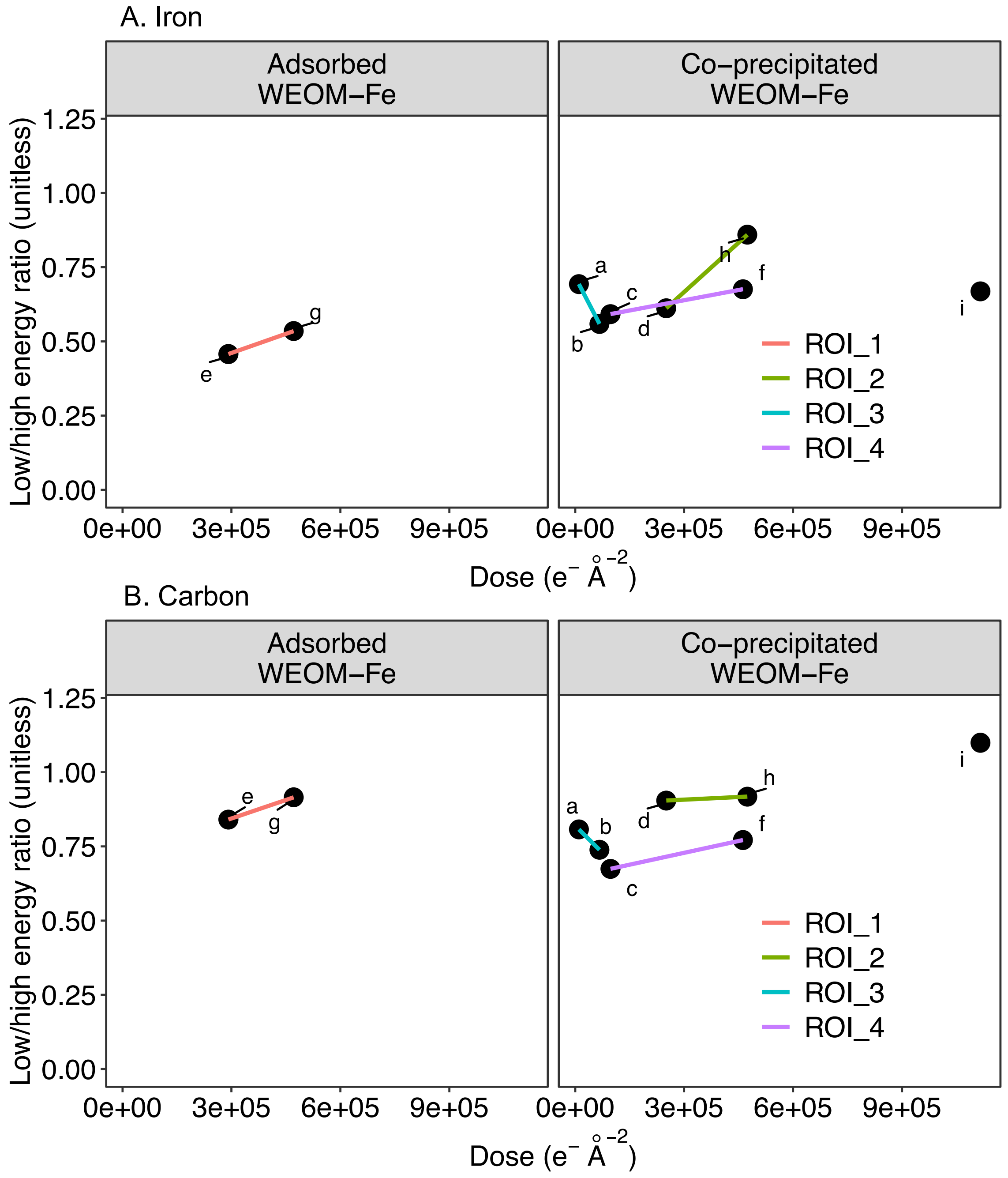

Supplementary Fig. A3.2. Change in ratio of lower-energy to higher-energy area under the curve (AUC) for (**A**) iron (Fe) L_3-edge and (**B**) carbon (C) K-edge average electron energy loss spectra. Lines connect measurements within the same region of interest (ROI). Corresponding spectra are shown in Supplementary Fig. A3.1. Spectra “a” through “i” correspond to measurement parameters described in Supplementary Table A4.4.

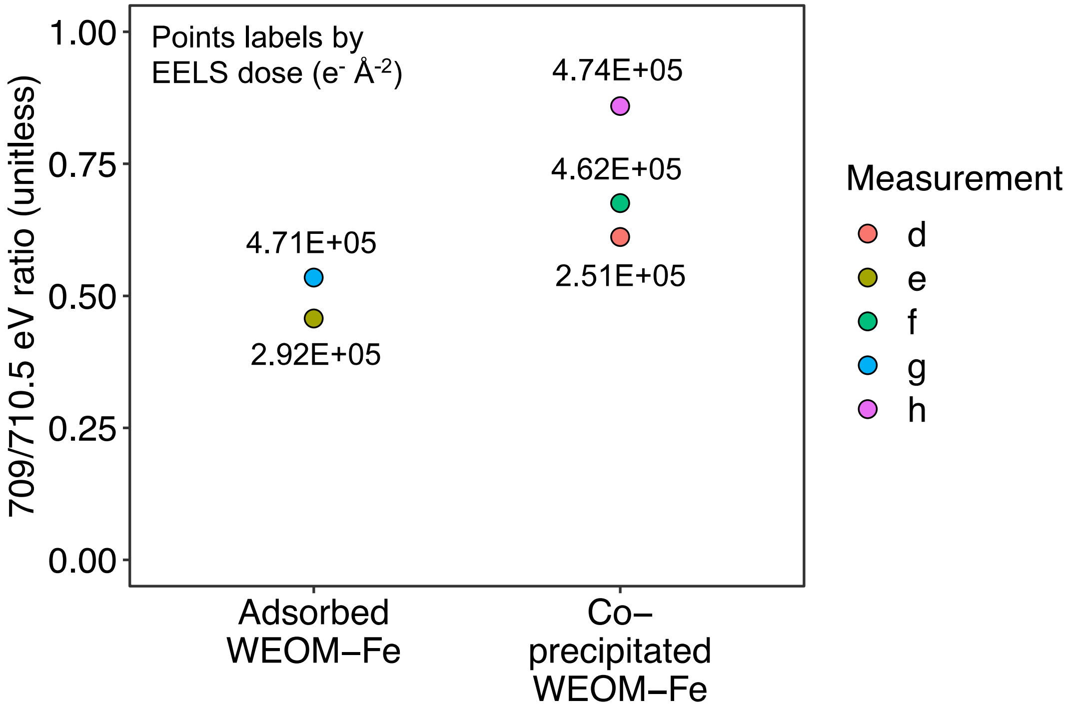

Supplementary Fig. A3.3. Relative change in ratio of lower-energy (~709 eV) to higher-energy (~710.5 eV) signal in the iron (Fe) L$_3$-edge between adsorbed and co-precipitated water extractable organic matter (WEOM)-Fe sample measurements at similar electron energy loss spectroscopy (EELS) dose. Spectra “d” through “h” correspond to measurement parameters described in Supplementary Table A4.4.

Adsorbed WEOM-Fe

A. Original ADF image

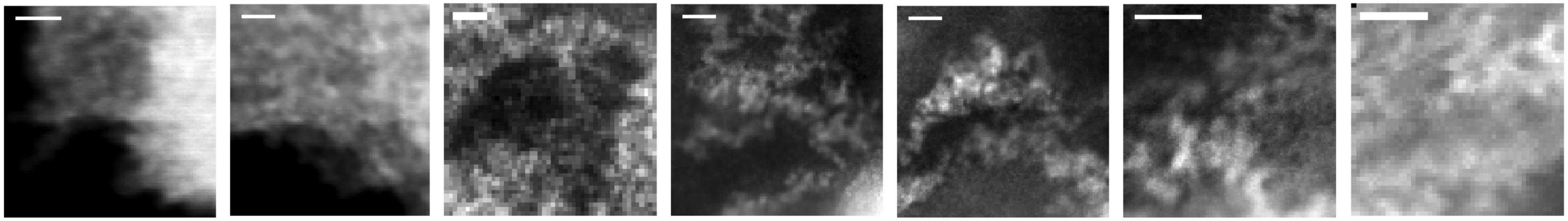

B. Iron (Fe) integrated area (vacuum filtered) with square region for Fe spatial analysis

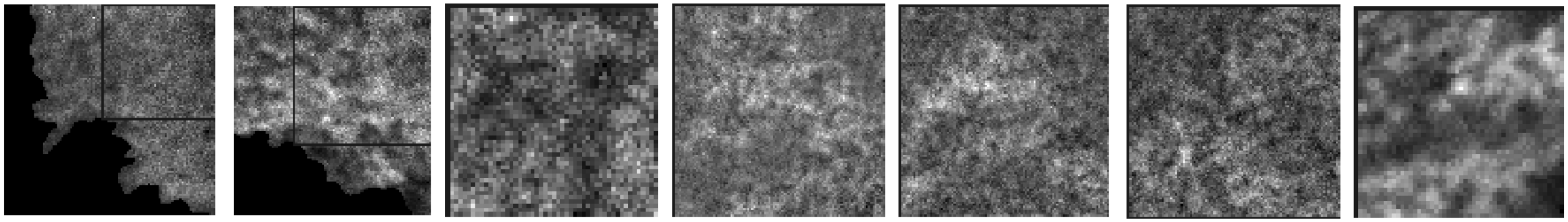

C. Binary Fe images (used for spatial statistics)

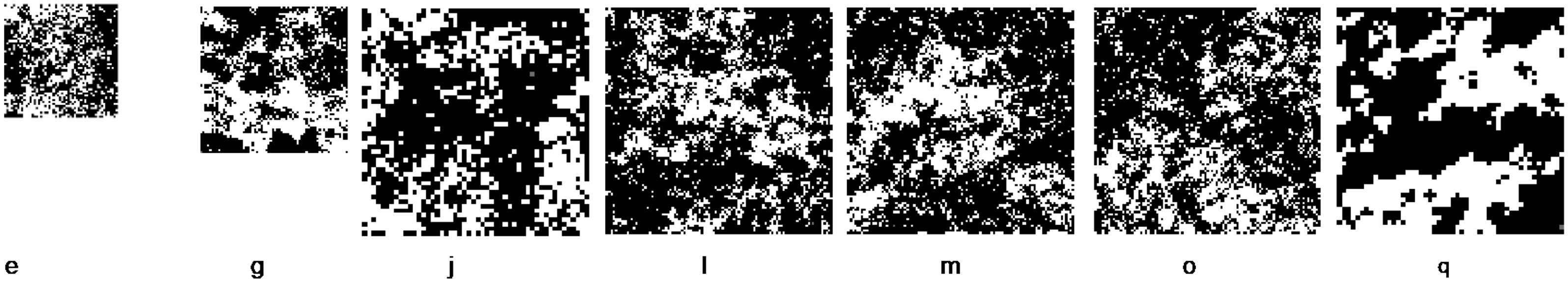

Supplementary Fig. A3.4. Image filtering and processing for iron (Fe) spatial statistics on adsorbed water-extractable organic matter (WEOM)-Fe images. **A**. Original annular dark field (ADF) scanning transmission electron microscopy (STEM) image. All scale bars = 10 nm. **B**. Integrated area of Fe $L_{2,3}$-edge with manual filter applied to remove vacuum area in image, if appropriate. Boxes show square region used for subsequent Fe spatial statistics, converted into binary images (shown in **C**). Lower-case letters correspond to measurements described in Supplementary Table A4.4.

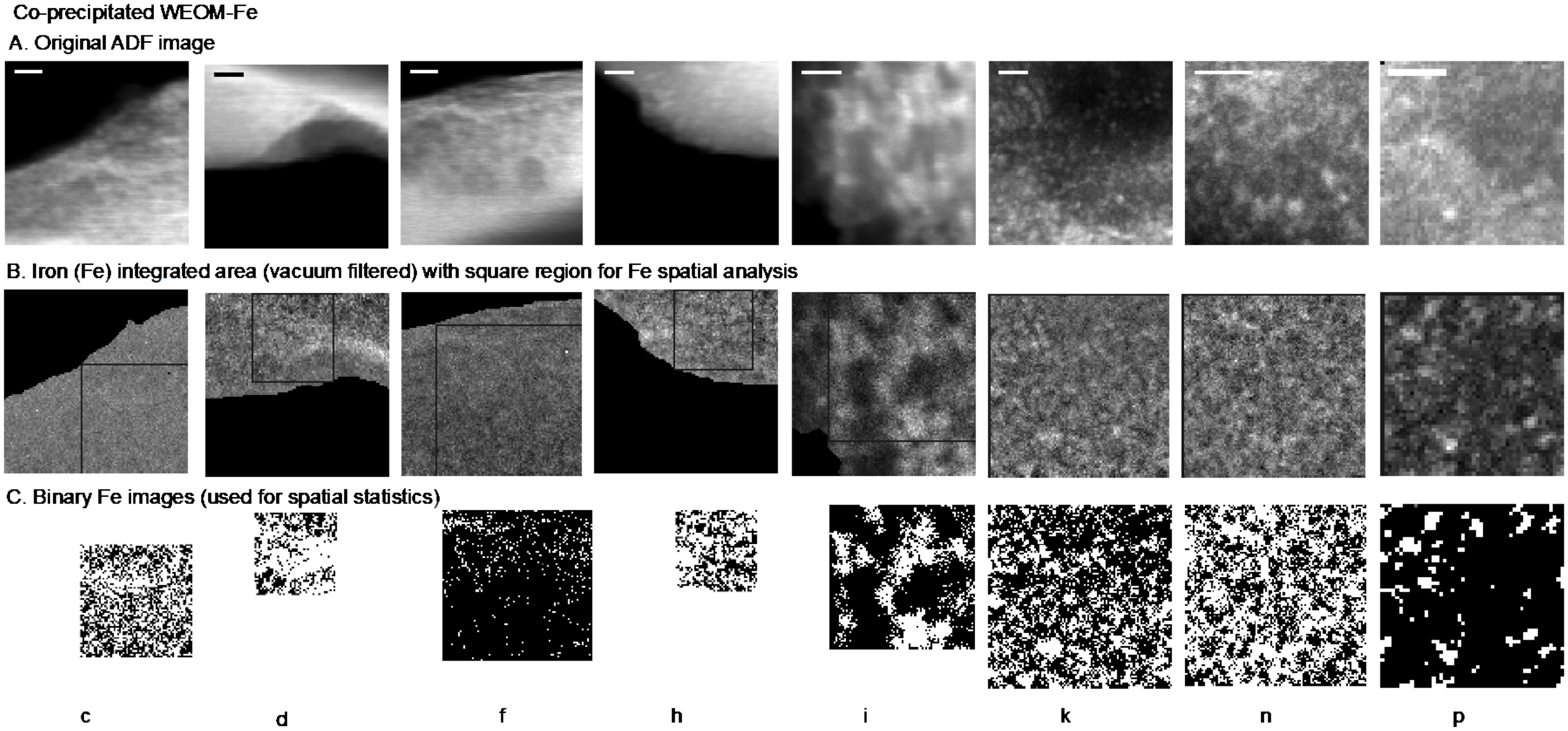

Supplementary Fig. A3.5. Image filtering and processing for iron (Fe) spatial statistics on co-precipitated water-extractable organic matter (WEOM)-Fe images. **A**. Original annular dark field (ADF) scanning transmission electron microscopy (STEM) image. All scale bars = 10 nm. **B**. Integrated area of Fe $L_{2,3}$-edge with manual filter applied to remove vacuum area in image, if appropriate. Boxes show square region used for subsequent Fe spatial statistics, converted into binary images (shown in **C**). Lower-case letters correspond to measurements described in Supplementary Table A4.4.

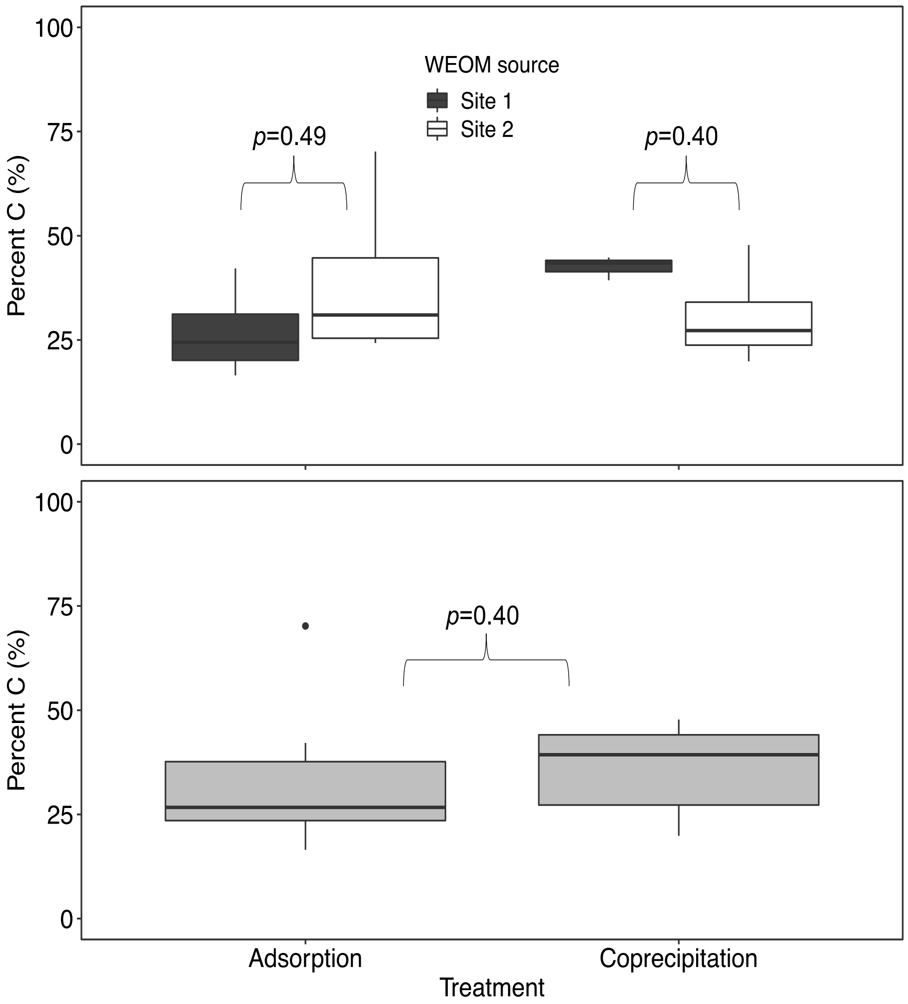

Supplementary Fig. A3.6. Total carbon (C) (%) for co-precipitate and adsorption samples at 10:1 C:Fe ratio, prepared with water-extractable organic matter (WEOM) derived from Site 1 and Site 2. No significant differences (at $\alpha = 0.1$) between Site 1 and Site 2 WEOM were detected (Wilcoxon Rank Sum $p > 0.4$). Pooled by WEOM source, the median carbon content was higher for co-precipitation but the difference was not significant (Wilcoxon Rank-Sum p=0.40) due to variation in adsorption C content. Lower and upper edges of boxes show first and third quartiles (25th and 75th percentiles) and lower and upper whiskers show the smallest and largest value no further than 1.5*interquartile range (IQR) of the box edges. Individual points beyond whiskers are considered outliers.

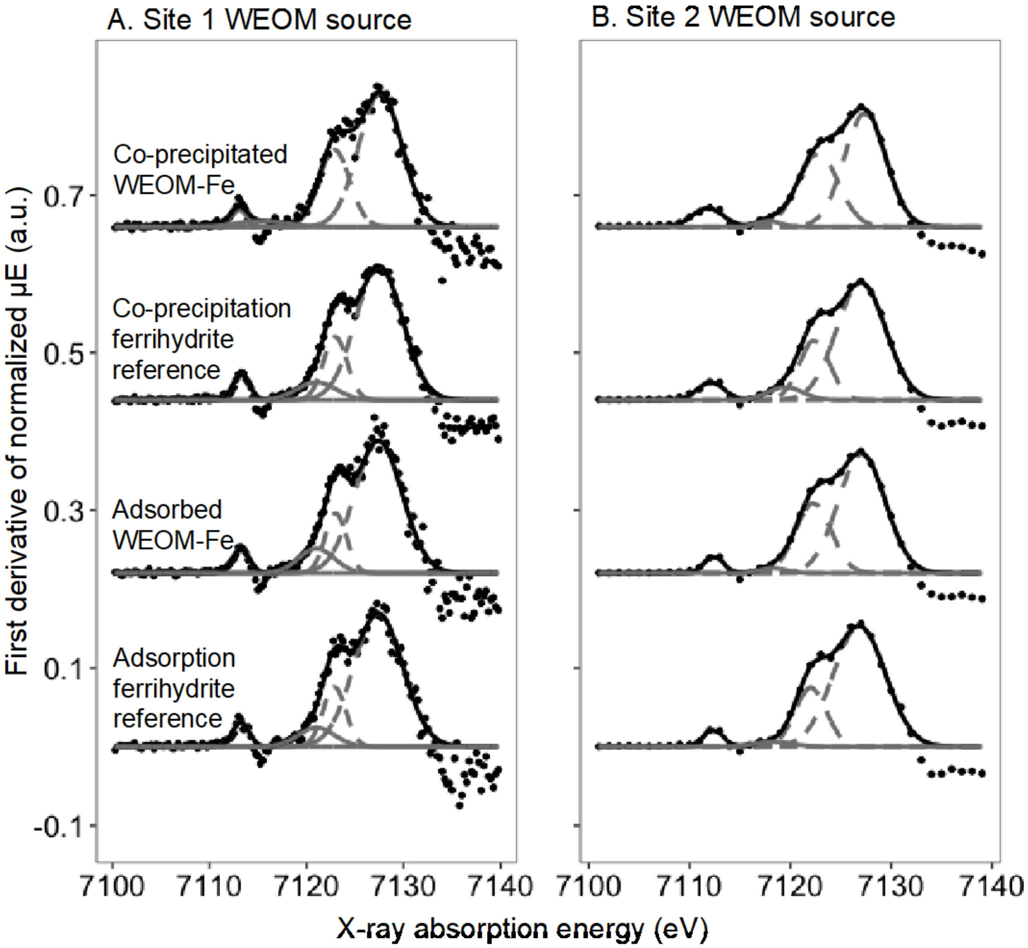

Supplementary Fig. A3.7. Iron (Fe) K-edge X-ray absorption near-edge structure (XANES) Gaussian fit results to determine relative contribution of the peak/shoulder ~7117-7120 eV associated with increasing Fe(II) content. The Gaussian function associated with this feature is shown as a solid grey line. Raw data are shown as points, other Gaussian functions in dashed grey, and the combined model fit in black (all spline curves).

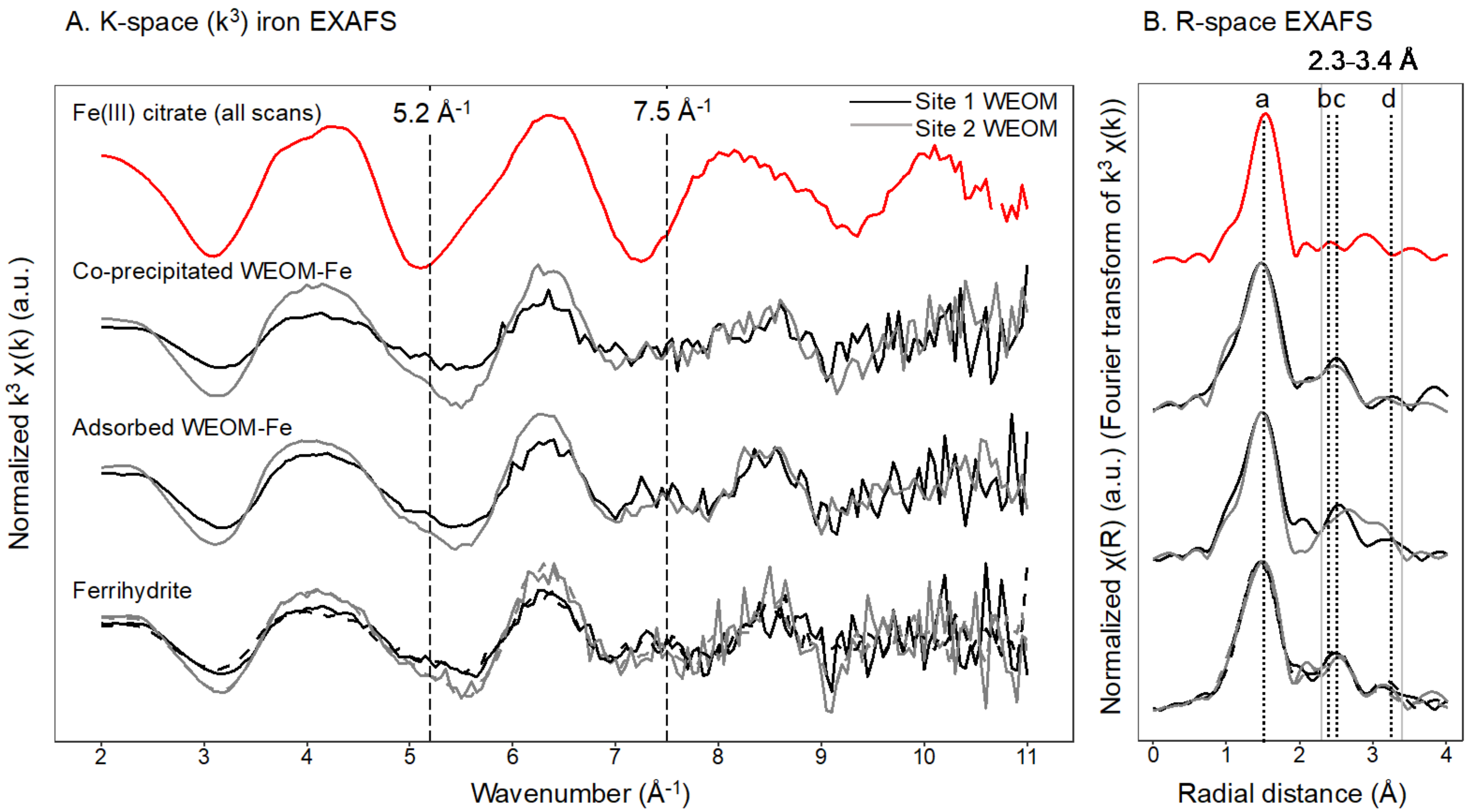

Supplementary Fig. A3.8. Iron (Fe) K-edge extended X-ray absorption fine structure (EXAFS) for co-precipitated and adsorbed WEOM-Fe. Reference ferrihydrite for adsorbed and co-precipitated samples is shown with solid and dotted lines, respectively. Adsorbed and co-precipitated samples generally follow the oscillation pattern of associated ferrihydrite reference materials. **A**. Normalized (max = 1) K-space (k^3-weighted) EXAFS, showing features at wavenumber ~5.2 and 7.5 Å^{-1} that are lost with increased C bonding in Fe (III) citrate (red line), corresponding to decreased high-shell backscatter signal (Chen et al., 2014). **B**. Inverse Fourier-transform (R-space) of k^3-weighted oscillations. Letters a-d correspond to Fe bonding environments assigned as follows: a = Fe-O, b = Fe-organic, and c and d = Fe-Fe (Chen et al., 2016). The shaded region (2.3-3.4 Å) represents general high-shell backscatter (features at wavenumber 5.2 and 7.5 Å^{-1} in **A**), lacking appreciable differences between co-precipitated and adsorbed WEOM-Fe and associated ferrihydrite standards. Additional standards are shown in Supplementary Fig. A3.9.

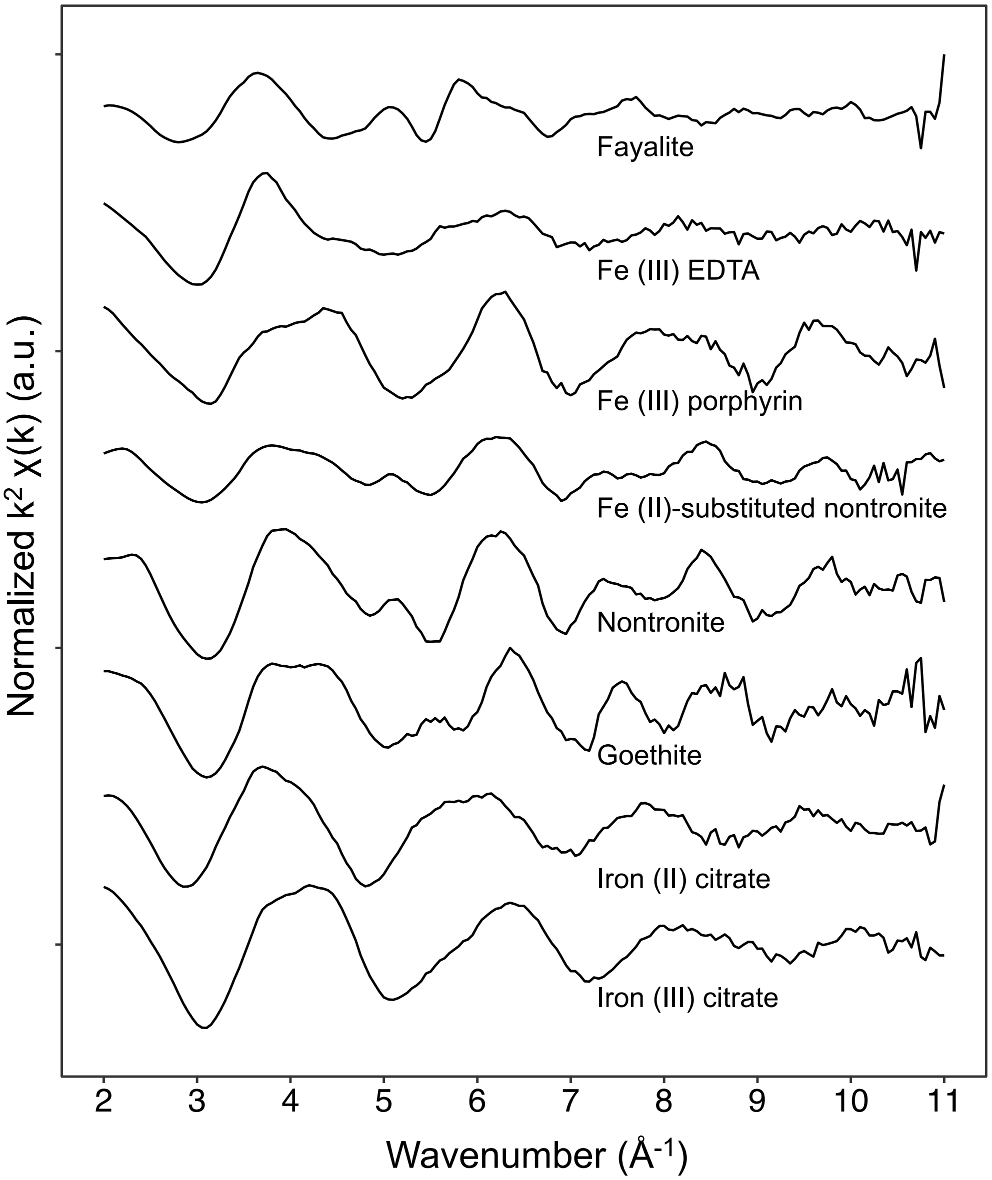

Supplementary Fig. A3.9. Normalized (max = 1) K-space (k^2-weighted) iron K-edge extended X-ray absorption fine structure (EXAFS) of standard reference materials. Iron (III) citrate, goethite, and nontronite are merged EXAFS spectra from two measured samples. The remaining spectra are derived from one measured sample.

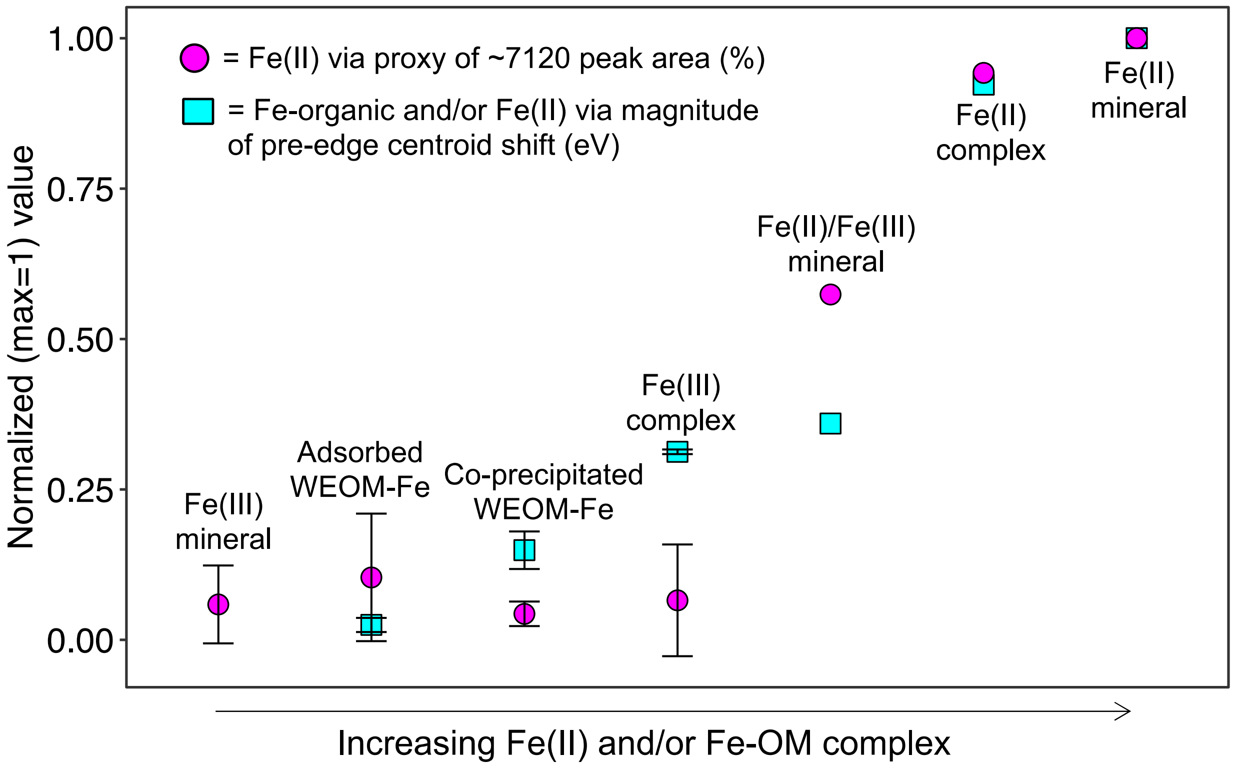

Supplementary Fig. A3.10. Visualization of combined changes in iron (Fe) K-edge X-ray absorption near edge structure (XANES), showing changes in ~7117-7120 eV peak area (% of Gaussian model) and centroid position for standard compounds and adsorbed vs. co-precipitated water-extractable organic matter (WEOM)-Fe materials normalized to 1. For Fe(II)/Fe(III) mineral, Fe(II) complex, and Fe(II) mineral points, values are for Fe(II)-substituted nontronite, iron (II) citrate, and fayalite, respectively. The average of two materials is shown for Fe(III) mineral (goethite and ferrihydrite), adsorbed and co-precipitated WEOM-Fe (Site 1 and Site 2 WEOM), and Fe(III) complex (iron (III) citrate and iron (III) EDTA) points (standard spectra are included in Inagaki et al. 2020). For the magnitude (absolute value) of the pre-edge centroid shift, the values for adsorption and co-precipitation were determined relative to the associated ferrihydrite reference, while the standard material shift was determined relative to the average of Fe(III) mineral positions (goethite and ferrihydrite).

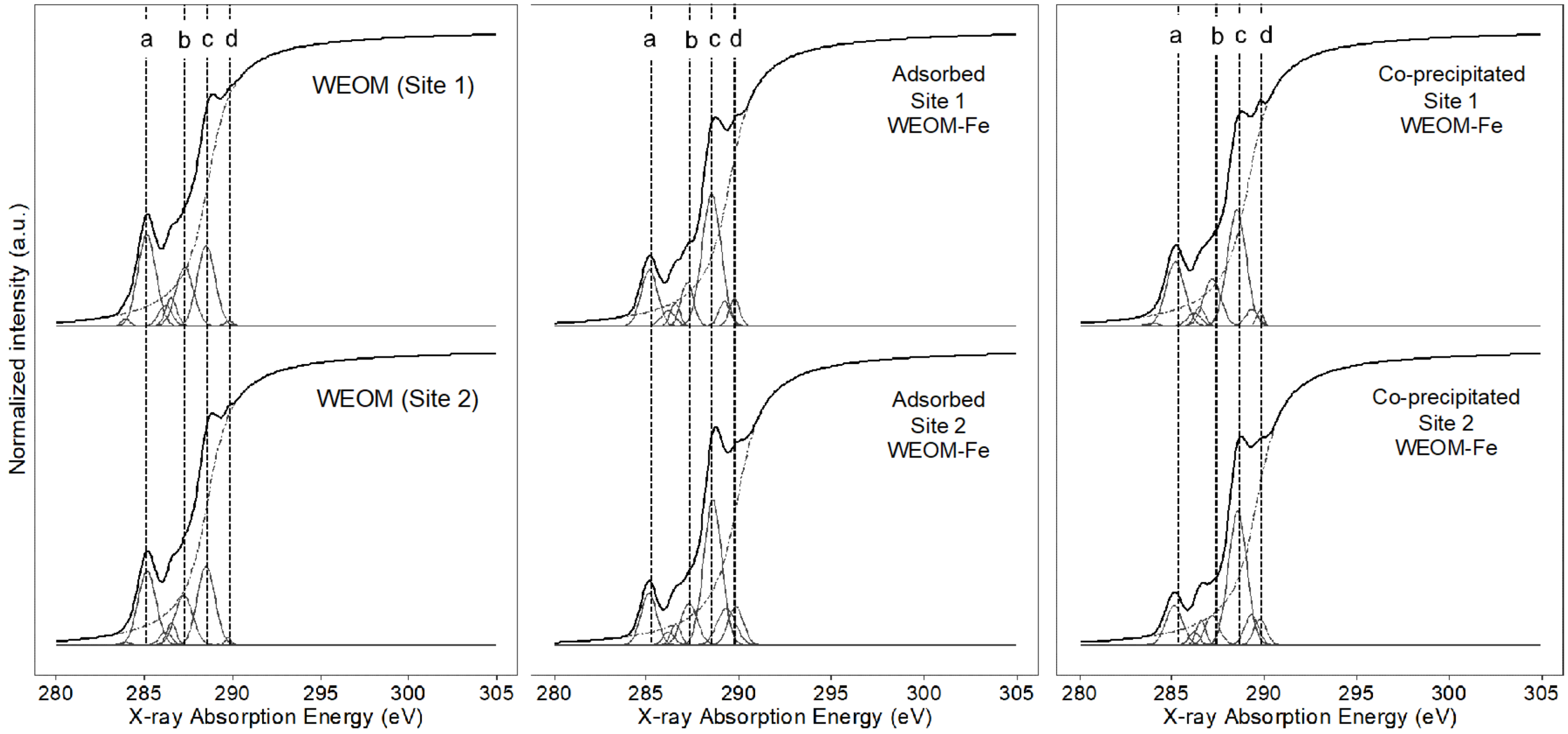

Supplementary Fig. A3.11. Gaussian and arctangent functions for deconvolution model of carbon (C) K-edge X-ray absorption near edge structure (XANES) for source water-extractable organic matter (WEOM) and adsorbed and co-precipitated WEOM-ferrihydrite complexes. Lines a, b, c, and d indicate spectral features at ~285.0, 287.5, 288.7, and 289.0 eV, corresponding to aromatic, aliphatic, carboxylic, and O-alkyl/carbonyl C functional groups, respectively.

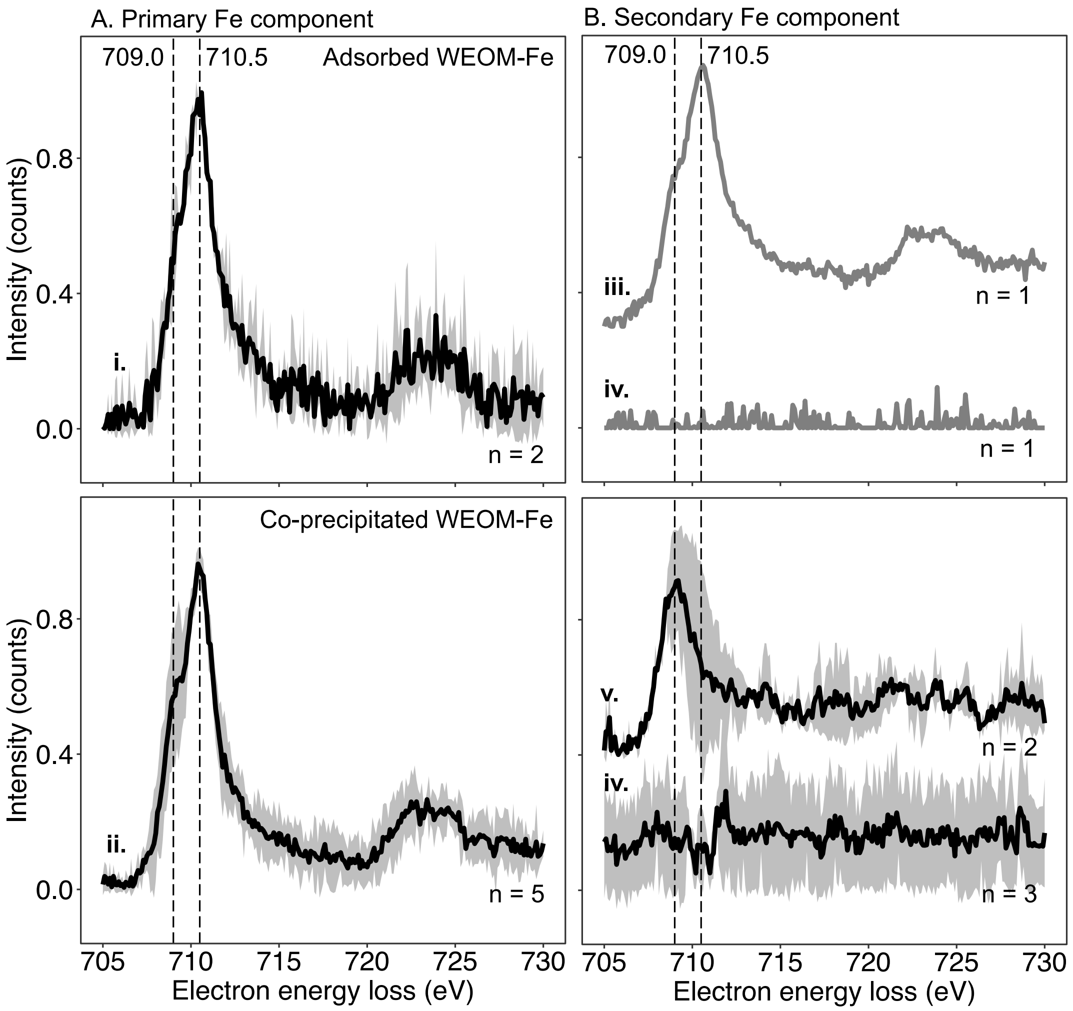

Supplementary Fig. A3.12. Iron (Fe) $L_{2,3}$-edge electron energy loss spectroscopy (EELS) multivariate curve resolution (MCR) outputs for water-extractable organic matter (WEOM) either co-precipitated with or adsorbed to Fe. Spectra are grouped by similar spectral features within sample types, and if n > 1 for each group, the average spectrum is shown (black line) with standard deviation (grey shaded region). **A**. All EELS measurements contained an Fe component with a primary L_3 edge postion at ~710.5 eV, associated with oxidized Fe(III). For co-precipitated WEOM-Fe (n = 5 EELS measurements) (**ii.**), a shoulder at lower energy (~709.0 eV) associated with increased Fe(II) was detected relative to adsorbed WEOM-Fe (n = 2 EELS measurements) (**i.**). **B**. For adsorbed WEOM-Fe, either no secondary component (**iv.**) or an Fe(III) component associated with thicker sample area (**iii.**) were detected (both n = 1 EELS measurement). For co-precipitated WEOM-Fe, either no secondary component (**iv.**) or an Fe(II) component with prominent shift to ~709.0 eV were detected (**v.**).

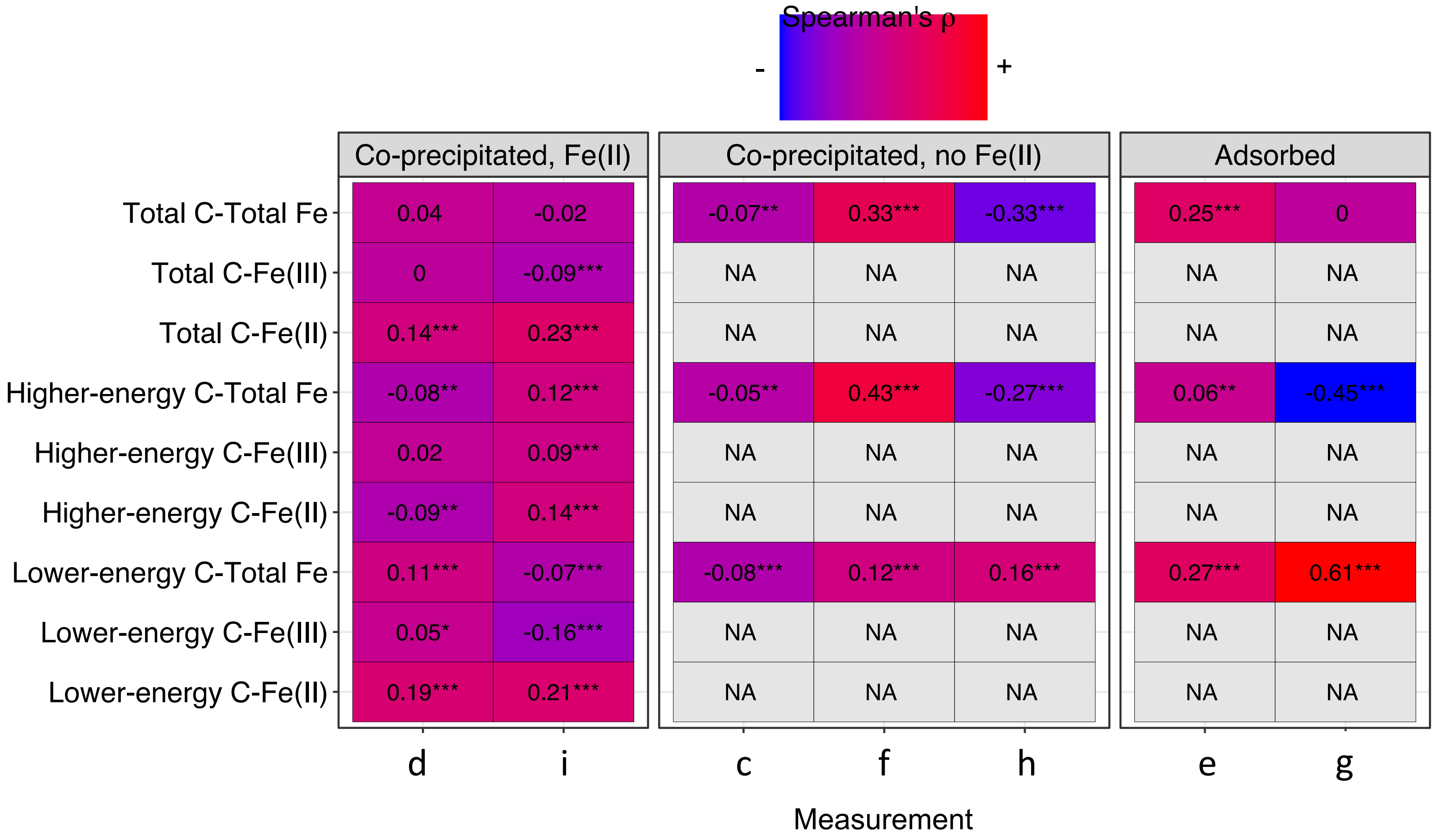

	Co-precipitated, Fe(II)		Co-precipitated, no Fe(II)			Adsorbed	
	d	i	c	f	h	e	g
Total C-Total Fe	0.04	-0.02	-0.07**	0.33***	-0.33***	0.25***	0
Total C-Fe(III)	0	-0.09***	NA	NA	NA	NA	NA
Total C-Fe(II)	0.14***	0.23***	NA	NA	NA	NA	NA
Higher-energy C-Total Fe	-0.08**	0.12***	-0.05**	0.43***	-0.27***	0.06**	-0.45***
Higher-energy C-Fe(III)	0.02	0.09***	NA	NA	NA	NA	NA
Higher-energy C-Fe(II)	-0.09**	0.14***	NA	NA	NA	NA	NA
Lower-energy C-Total Fe	0.11***	-0.07***	-0.08***	0.12***	0.16***	0.27***	0.61***
Lower-energy C-Fe(III)	0.05*	-0.16***	NA	NA	NA	NA	NA
Lower-energy C-Fe(II)	0.19***	0.21***	NA	NA	NA	NA	NA

Supplementary Fig. A3.13. Spatial correlations (Spearman's ρ estimates) among carbon (C) and iron (Fe) electron energy loss spectroscopy components identified with multivariate curve resolution for adsorbed and co-precipitated water-extractable organic matter (WEOM)-Fe samples. For adsorbed and a subset of co-precipitated WEOM-Fe samples, no meaningful reduced Fe(II) component was detected (Supplementary Fig. A3.11), so only spatial correlations between C forms (non-oxidized, oxidized, and total C) and total Fe are shown. Lower-case letters correspond to individual measurements (defined in Supplementary Table A4.4). *, **, and *** symbols indicate Spearman Rank Test *p* < 0.1, 0.05, and 0.001, respectively.

A4. Supplementary Tables

Supplementary Table A4.1. Carbon (C) K-edge X-ray absorption near-edge structure (XANES) deconvolution model parameters, modified from Heymann et al. (2011).

Description	Function in model	Bond(s)	Transition	Center (eV)	Center range (+/- eV)	Height (a.u.)	FWHM (eV)	FWHM range (eV)	Inflection	Vertical position (a.u.)
Arctangent Edge step	Atan	NA (total C)	NA (total C)	290.00	Floating	1 (fixed)	NA	NA	0.335 (fixed)	0.5 (fixed)
Aromatic Quinone	G1	C=O	1 s-pi*	283.75	0.2*sin(~0)	√ ~0.4	0.4	0.2*sin(~0)	NA	NA
Aromatic	G2	C=C	1 s-pi*	285.20	0.2*sin(~0)	√ ~0.4	0.4	0.2*sin(~0)	NA	NA
Aromatic	G3	C=O	1 s-pi*	286.00	0.2*sin(~0)	√ ~0.4	0.4	0.2*sin(~0)	NA	NA
Aromatic w/substituent	G4	C=C-OH C=O R-(C=O)-R'	1 s-pi*	286.70	0.2*sin(~0)	√~0.4	0.4	0.2*sin(~0)	NA	NA
Alkyl	G5	C-H	1s-pi*	287.30	0.2*sin(~0)	√~0.4	0.4	0.2*sin(~0)	NA	NA
Carboxylic	G6	R-COOH COO C=O	1s-3p/sigma*	288.70	0.2*sin(~0)	√~0.4	0.4	0.2*sin(~0)	NA NA	NA NA
O-alkyl	G7	C-OH	1s-pi*	289.35	0.1*sin(~0)	√~0.4	0.4	0.2*sin(~0)	NA	NA
O-alkyl /carbonyl	G8	COO-	1s-pi*	289.85	0.1*sin(~0)	√~0.4	0.4	0.2*sin(~0)	NA	NA

Supplementary Table A4.2. Carbon K-edge X-ray absorption near-edge structure (XANES) deconvolution results for water-extractable matter (WEOM) samples derived from Site 1 and Site 2 organic (Oa) horizons, and for WEOM-ferrihydrite adsorption and co-precipitation solids prepared at a 10:1 C/Fe ratio.

	Site 2 source WEOM (R^2 = 0.994)					Site 1 source WEOM (R^2 = 0.994)				
Gaussian	Center (eV)	Height (a.u.)	Area (a.u.)	FWHM (eV)	Proportion (%)	Center (eV)	Height (a.u.)	Area (a.u.)	FWHM (eV)	Proportion (%)
G1	283.95	0.01	0.01	0.61	0.64	283.95	0.02	0.02	0.59	1.33
G2	285.16	0.26	0.33	1.2	32.91	285.14	0.32	0.40	1.20	34.07
G3	286.20	0.05	0.04	0.78	3.77	286.20	0.07	0.07	0.92	5.86
G4	286.54	0.08	0.05	0.61	5.16	286.52	0.10	0.08	0.72	6.43
G5	287.24	0.17	0.22	1.19	21.87	287.29	0.20	0.26	1.19	21.63
G6	288.50	0.27	0.34	1.17	34.47	288.51	0.28	0.35	1.19	29.69
G7	289.17	0.00	0.00	0.46	0.07	289.48	0.00	0.00	0.69	0.06
G8	289.76	0.03	0.01	0.41	1.12	289.78	0.02	0.01	0.56	0.93
	Co-precipitate (Site 2 WEOM) (R^2 = 0.997)					Co-precipitate (Site 1 WEOM) (R^2 = 0.996)				
G1	283.63	0.00	0.00	0.83	0.00	283.95	0.01	0.01	0.78	0.71
G2	285.12	0.14	0.15	1.06	14.15	285.18	0.22	0.27	1.16	24.03
G3	286.20	0.05	0.03	0.66	3.02	286.20	0.05	0.04	0.89	3.85
G4	286.58	0.09	0.05	0.59	5.00	286.50	0.07	0.05	0.66	4.10
G5	287.18	0.10	0.10	0.90	9.02	287.18	0.16	0.19	1.09	16.65
G6	288.55	0.46	0.57	1.16	52.79	288.50	0.40	0.50	1.18	44.27
G7	289.30	0.11	0.10	0.85	8.97	289.32	0.06	0.05	0.79	4.29
G8	289.77	0.09	0.08	0.79	7.06	289.75	0.06	0.02	0.40	2.10
	Adsorption complex (Site 2 WEOM) (R^2 = 0.997)					Adsorption complex (Site 1 WEOM) (R^2 = 0.996)				
G1	283.95	0.00	0.00	0.47	0.03	283.95	0.00	0.00	0.48	0.04
G2	285.12	0.18	0.19	0.98	14.13	285.15	0.19	0.21	1.02	18.39
G3	286.19	0.05	0.04	0.73	2.63	286.18	0.05	0.05	0.89	4.29
G4	286.58	0.07	0.05	0.62	3.61	286.54	0.08	0.05	0.59	4.39
G5	287.30	0.14	0.16	1.04	11.91	287.19	0.15	0.13	0.79	11.02
G6	288.57	0.50	0.61	1.14	45.48	288.50	0.46	0.58	1.20	50.64
G7	289.31	0.13	0.16	1.18	11.91	289.19	0.09	0.06	0.70	5.58
G8	289.81	0.13	0.14	0.97	10.29	289.75	0.10	0.06	0.64	5.65

Supplementary Table A4.3. Summary of carbon K-edge X-ray absorption near-edge structure (XANES) deconvolution results for standard C compounds. Major XANES features associated with the dominant functional groups for the standard materials are noted with (*).

Standard	Gaussian	Center (eV)	Height (a.u.)	Area (a.u.)	FWHM (eV)	Proportion (%)
Salicylic acid 2-Hydroxybenzoic acid $C_7H_6O_3$ Fit R^2 = 0.990	G1	283.63	0.00	0.00	0.83	0.00
	G2	285.12	0.14	0.15	1.06	14.15*
	G3	286.20	0.05	0.03	0.66	3.02
	G4	286.58	0.09	0.05	0.59	5.00
	G5	287.18	0.10	0.10	0.90	9.02
	G6	288.55	0.46	0.57	1.16	52.79*
	G7	289.30	0.11	0.10	0.85	8.97
	G8	289.77	0.09	0.08	0.79	7.06
Citric acid 2-hydroxypropane-1,2,3-tricarboxylic acid $C_6H_8O_7$ Fit R^2 = 0.996	G1	283.71	0.00	0.00	1.16	0.00
	G2	285.11	0.02	0.01	0.41	0.73
	G3	286.15	0.00	0.00	0.49	0.18
	G4	286.77	0.13	0.06	0.43	4.66
	G5	287.41	0.17	0.14	0.78	11.27
	G6	288.60	0.63	0.63	0.94	49.34*
	G7	289.17	0.28	0.26	0.89	20.67*
	G8	289.95	0.18	0.17	0.89	13.15*
Sucrose (2R,3R,4S,5S,6R)-2-[(2S,3S,4S,5R)-3,4-dihydroxy-2,5-bis(hydroxymethyl)oxolan-2-yl]oxy-6-(hydroxymethyl)oxane-3,4,5-triol $C_{12}H_{22}O_{11}$ Fit R^2 = 0.994	G1	283.60	0.00	0.00	0.73	0.00
	G2	285.15	0.02	0.01	0.41	1.23
	G3	286.09	0.02	0.02	0.68	2.32
	G4	286.64	0.05	0.02	0.41	3.09
	G5	287.20	0.00	0.00	0.41	0.05
	G6	288.81	0.33	0.23	0.66	33.16
	G7	289.24	0.30	0.22	0.70	31.69*
	G8	289.85	0.24	0.20	0.78	28.46*

Supplementary Table A4.4. Acquisition parameters for electron energy loss spectroscopy (EELS) measurements of co-precipitated and adsorbed water-extractable organic matter (WEOM)-iron samples. MCR = multivariate curve resolution. * = from Possinger et al. (2020b).

Measurement	EELS data type	WEOM source	Treatment	Instrument conditions	Magnification (Mx)	EELS acquisition time (s)	Current (nA)	Dose (e^{-} Å^{-2})
a*	FOV scan	Site 2	Co-precipitated	Cryo	0.64	0.01	0.16	1.03E+04
b*	FOV scan	Site 2	Co-precipitated	Cryo	0.64	0.01	0.16	6.69E+04
c	Map	Site 2	Co-precipitated	Cryo	1.30	0.01	0.025	9.73E+04
d	Map	Site 2	Co-precipitated	Cryo	1.30	0.01	0.075	2.51E+05
e	Map	Site 2	Adsorbed	Cryo	1.80	0.01	0.042	2.92E+05
f	Map	Site 2	Co-precipitated	Cryo	1.30	0.05	0.025	4.62E+05
g	Map	Site 2	Adsorbed	Cryo	1.30	0.01	0.130	4.71E+05
h	Map	Site 2	Co-precipitated	Cryo	1.30	0.01	0.125	4.74E+05
i	Map	Site 2	Co-precipitated	Cryo	1.80	0.01	0.160	1.12E+06
j	Map	Site 1	Adsorbed	Not cryo	2.55	0.001	0.025	1.37E+04
k	Map	Site 1	Co-precipitated	Not cryo	1.30	0.005	0.025	5.20E+04
l	Map	Site 1	Adsorbed	Not cryo	2.55	0.001	0.025	5.20E+04
m	Map	Site 1	Adsorbed	Not cryo	1.30	0.001	0.025	5.20E+04
n	Map	Site 1	Co-precipitated	Not cryo	1.30	0.001	0.025	1.99E+05
o	Map	Site 1	Adsorbed	Not cryo	1.30	0.001	0.025	2.01E+05
p	Map	Site 1	Co-precipitated	Not cryo	2.55	0.200	0.025	1.62E+06
q	Map	Site 1	Adsorbed	Not cryo	2.55	0.200	0.025	2.20E+06

Supplementary Table A4.5. Comparison of carbon (C) K-edge and iron (Fe) L$_{2,3}$-edge electron energy loss spectral region areas between compositionally similar regions in a co-precipitated sample (i.e., with detected reduced Fe(II) and similar C-Fe(II) spatial relationships). Area under the curve estimates are for aromatic C (284.5-285.5 eV), substituted aromatic C (286.0-287.0 eV), aliphatic C (287.0-287.5 eV), carboxylic C (287.8-289.0 eV), reduced Fe(II) (707.0-709.75 eV) and oxidized Fe(III) (709.75-712.5 eV) spectral regions.

Measurement	Dose (e^{-} Å^{-2})	Estimated area under the curve					
		Carboxylic	Aromatic	Subst. aromatic	Alkyl	Fe(II)	Fe(III)
d	2.51E+05	0.032	0.017	0.023	0.012	0.157	0.258
i	1.12E+06	0.031	0.021	0.029	0.014	0.195	0.292
Difference (%)		4.05	20.98	26.33	17.86	23.82	13.26